



High temperature reduction dramatically promotes Pd/TiO₂ catalyst for ambient formaldehyde oxidation

Yaobin Li^a, Changbin Zhang^{b,c,**}, Jinzhu Ma^{b,c,d}, Min Chen^{b,c}, Hua Deng^a, Hong He^{a,b,c,d,*}

^a Key Laboratory of Urban Pollutant Conversion, Institute of Urban Environment, Chinese Academy of Sciences, Xiamen 361021, China

^b State Key Joint Laboratory of Environment Simulation and Pollution Control, Research Center for Eco-environmental Sciences, Chinese Academy of Sciences, Beijing 100085, China

^c University of Chinese Academy of Sciences, Beijing 100049, China

^d Center for Excellence in Regional Atmospheric Environment, Institute of Urban Environment, Chinese Academy of Sciences, Xiamen 361021, China

ARTICLE INFO

Article history:

Received 5 January 2017

Received in revised form 6 June 2017

Accepted 8 June 2017

Available online 9 June 2017

Keywords:

Formaldehyde

Pd/TiO₂

Low/high temperature reduction

SMSI

Oxygen vacancies

Reaction pathway

ABSTRACT

High temperature reduction generally induces the sintering of supported noble metals, therefore resulting in a negative effect on their performance. Here, we show that high temperature reduction was able to dramatically increase the activity of Pd/TiO₂ for ambient HCHO oxidation. We prepared a Pd/TiO₂ catalyst and pre-reduced it with H₂ at low temperature (300 °C) and high temperature (450 °C), respectively, and then tested the activity for HCHO oxidation at ambient temperature. The Pd/TiO₂-450R catalyst showed a much better performance than Pd/TiO₂-300R at room temperature. 100% HCHO conversion could be obtained on the Pd/TiO₂-450R catalyst at a GHSV of 95000 h⁻¹ and 140 ppm inlet HCHO. The catalysts were then characterized by using Brunauer-Emmett-Teller (BET), X-ray diffraction (XRD), High-angle annular dark-field scanning transmission electron microscopy (HAADF-STEM) and other methods. The results indicate that high temperature reduction could induce the strong metal-support interaction (SMSI), decreasing the surface Pd particle size by partially encapsulating and trapping Pd clusters with TiO₂, and also could produce more oxygen vacancies, beneficial to the activation of O₂ and formation of surface OH groups, opening a more effective pathway for ambient HCHO oxidation. Therefore, the Pd/TiO₂-450R catalyst demonstrated high activity for ambient HCHO oxidation.

© 2017 Elsevier B.V. All rights reserved.

1. Introduction

Increasing numbers of people are suffering from Sick Building Syndrome (SBS) due to the fact that we are spending more time in airtight houses. Formaldehyde (HCHO) is one of the most common and noxious gaseous pollutants [1]. Long-term exposure to indoor air containing HCHO, even at very low ppm levels, may lead to serious health problems including nasal tumors, irritation of the mucous membranes of the eyes and respiratory tract, skin irritation, decreased concentration, and weakened immunity [2]. Therefore,

to reduce public health risk, the effective abatement of indoor air HCHO is urgently needed.

Conventional methods to remove HCHO include adsorption, photo-catalysis, plasma technology and catalytic oxidation [3–6]. Due to its high effectiveness in complete oxidation of HCHO into harmless CO₂ and H₂O without any secondary pollution, catalytic oxidation is regarded as the most promising method for HCHO removal [7,8]. Compared with metal oxide catalysts (Ag, Mn, Co) [9–12], supported noble metal (Pt, Au, Pd) catalysts are considered to be especially suitable for indoor HCHO elimination because of their excellent performance in HCHO oxidation at room temperature [13–28]. However, the high cost of Pt- or Au-based catalysts limits their wide application. By contrast, Pd-based catalysts are much less expensive and thus have the potential for more extensive application in indoor air HCHO purification.

It has been reported that the performance of Pd-based catalysts is closely related to the reduction treatment used [17], presence of metal promoters [19,22,24] and morphology of the support [29], etc. In particular, the reduction temperature can have great effects

* Corresponding author at: Key Laboratory of Urban Pollutant Conversion, Institute of Urban Environment, Chinese Academy of Sciences, Xiamen 361021, China.

** Corresponding author at: State Key Joint Laboratory of Environment Simulation and Pollution Control, Research Center for Eco-environmental Sciences, Chinese Academy of Sciences, Beijing, 100085, China.

E-mail addresses: cbzhang@rcees.ac.cn (C. Zhang), hhe@iue.ac.cn, honghe@rcees.ac.cn (H. He).

on the activity of Pd-based catalysts for some reactions, such as the CO/H₂ reaction [30], hydrogenation of acetylene and vinylacetylene [31], methane [32] and o-xylene [33] oxidation, etc. Generally, a high reduction temperature may induce sintering of supported metals, which is detrimental to catalyst performance. [31,32,34] However, for reducible oxide supports (such as TiO₂, CeO₂ and Co₃O₄, etc.), high temperature treatment may induce the strong metal-support interaction (SMSI), which may possibly result in the encapsulation of metal clusters and increase their sintering resistance, thus having a positive effect on catalyst performance. [35] In addition, TiO₂ is liable to form surface oxygen vacancies with high temperature reduction, leading to dissociation of chemisorbed H₂O to form surface hydroxyl, [36] which has been found to play an important role in the HCHO oxidation reaction [13]. Considering the above information, it is worth exploring the influence of reduction temperature on Pd/TiO₂ catalysts for HCHO oxidation.

In this study, a Pd/TiO₂ catalyst was prepared and pre-reduced with H₂ at low temperature (300 °C) and high temperature (450 °C) before being tested for HCHO oxidation at ambient temperature. It was found that the Pd/TiO₂ catalyst reduced at 450 °C was much more active for HCHO oxidation than that reduced at 300 °C, and 100% conversion of 140 ppm HCHO at a GHSV of 95000 h⁻¹ could be reached using Pd/TiO₂-450R at room temperature. The catalysts were then characterized by X-ray diffraction (XRD), Brunauer-Emmett-Teller (BET), CO chemisorption, High-angle annular dark-field scanning transmission electron microscopy (HAADF-STEM), Temperature programmed reduction by H₂ (H₂-TPR), X-ray photoelectron spectroscopy (XPS), *in situ* Diffuse Reflectance Infrared Fourier Transform Spectroscopy (*in situ* DRIFT) and Temperature-programmed desorption by HCHO (HCHO-TPD) methods. Based on the results, the mechanism of the promotion effect of high temperature reduction is discussed and elucidated.

2. Experimental

2.1. Catalyst preparation

1 wt.% Pd/TiO₂ was prepared by impregnation of TiO₂ with aqueous Pd(NO₃)₂, according to our previous study [19,22]. Before activity testing and characterization, the samples were reduced with H₂ at 300 °C and 450 °C for 1 h, and denoted as Pd/TiO₂-300R and Pd/TiO₂-450R respectively.

2.2. Catalyst characterization

X-ray diffraction (XRD), Brunauer-Emmett-Teller (BET) analysis, CO pulsed chemisorption, H₂ temperature-programmed reduction (H₂-TPR), X-ray photoelectron spectroscopy (XPS) and O₂ temperature-programmed desorption (O₂-TPD) were carried out according to our previous work [19]. Before the characterization, the Pd/TiO₂ catalyst was first reduced with H₂ at 300 °C or 450 °C for 1 h followed by purging with He for 30 min and then the system was cooled down to 25 °C. Typically, for H₂-TPR, the Pd/TiO₂-300R/450R catalysts were pretreated by 10% O₂/He for 30 min followed by purging with He for 30 min at 25 °C. Then, the system was cooled down to -50 °C followed by reduction with 10% H₂/Ar from -50 to 100 °C at a rate of 10 °C/min.

High-angle annular dark-field scanning transmission electron microscopy (HAADF-STEM) was performed on a JEOL JEM-ARM 200F with Cs-corrected probe operated at 200 kV. The surface-weighted particle size d_s was calculated according to the previous work [37].

Fourier transform infrared (FTIR) spectra were recorded at room temperature on a Thermo Fisher IS 50 spectrometer

equipped with an MCT detector. Samples were loaded into an infrared cell equipped with ZnSn windows. The scan region was 4000–1000 cm⁻¹ (16 scans, resolution of 0.5 cm⁻¹). The samples were also pre-reduced with H₂ at 300 °C or 450 °C for 1 h, followed by purging with He for 30 min at 300 °C to desorb H₂ and H₂O. Then, the system was cooled down to room temperature before introduction of reactants. To investigate surface hydroxyl groups of samples, FTIR spectra of dry Pd/TiO₂-300R/450R catalysts were recorded according to the previous work [25,27]. Typically, a Bruker Tensor 27 FTIR Spectrometer was used to collect FTIR spectra. About 2 mg samples was mixed with 100 mg KBr followed by drying under a heat lamp, then the mixture was pressed into a transparent pellet die before FTIR tests.

HCHO temperature program desorption (HCHO-TPD) was performed on a Micromeritics AutoChem II 2920 apparatus equipped with a MS detector. The apparatus is also equipped with a vapor generator, in which some paraformaldehyde was loaded. In HCHO-TPD experiment, HCHO gas was generated by heating the vapor generator at around 45 °C, and the helium gas carried the HCHO gas into the reactor for HCHO adsorption on catalysts. The catalysts (~100 mg) were first pre-reduced with 50 mL 10% H₂/Ar at 300 °C or 450 °C for 1 h, followed by flushing in 50 mL He flow at 300 °C for 30 min. Subsequently, the system was cooled down to 25 °C and the gas switched to 50 mL 10% O₂/H₂ containing 40% RH for 30 min, followed by He purge for 30 min. After that, the catalyst was further cooled down to 0 °C and HCHO adsorption was carried out for 1 h, followed by He purge for 30 min, then HCHO-TPD was conducted in He from 0 to 400 °C at a rate of 10 °C/min.

2.3. Catalyst activity testing

Catalyst activity testing for HCHO oxidation and carbon balance calculation were performed according to our previous works [19,38]. Typically, before activity testing, the catalysts were pre-reduced with H₂ flow at 300 or 450 °C for 1 h, followed by He flow purge at 300 °C for 30 min, and then cooled down to room temperature. The activity duration testing was performed under a harsher condition with 300 ppm HCHO. Conversion of HCHO (γ , %) was calculated as follows:

$$\gamma = \frac{[\text{HCHO}]_{\text{in}} - [\text{HCHO}]_{\text{out}}}{[\text{HCHO}]_{\text{in}}} \times 100\%$$

Where [HCHO]_{in} and [HCHO]_{out} are inlet and outlet HCHO concentration, respectively. Moreover, the carbon balance was also calculated and the results are presented in Table S1 (supporting information).

Turnover frequency (TOF, s⁻¹) was obtained based on a separate experiment where the conversion of HCHO was kept below 30% by varying the inlet HCHO concentration and GHSV, with negligible heat and mass-transfer effects and TOF was calculated according to the following equation [39]:

$$\text{TOF} = \frac{\dot{n}_{\text{HCHO}}}{\dot{n}_{\text{Pd}}} = \frac{[\text{HCHO}]_{\text{in}} \cdot \gamma \cdot V/R_g}{m_{\text{cat.}} \cdot \omega_{\text{Pd}} \cdot D_{\text{Pd}}/M_{\text{Pd}}}$$

Where the parameters are the molar weight of consumed HCHO per second (n'_{HCHO} , mol s⁻¹), molar weight of Pd exposed on TiO₂ surface (n_{Pd} , mol), initial inlet concentration of HCHO ([HCHO]_{in}, ppm), total flow rate (V, L s⁻¹), molar volume of gas at 25 °C and 101 kPa (R_g, 24.5 L mol⁻¹), weight of catalyst (m_{cat.}, g), loading percentage of Pd (ω_{Pd} , %), Pd dispersion (D_{Pd}, %) and molecular mass of Pd (M_{Pd}, gmol⁻¹), respectively.

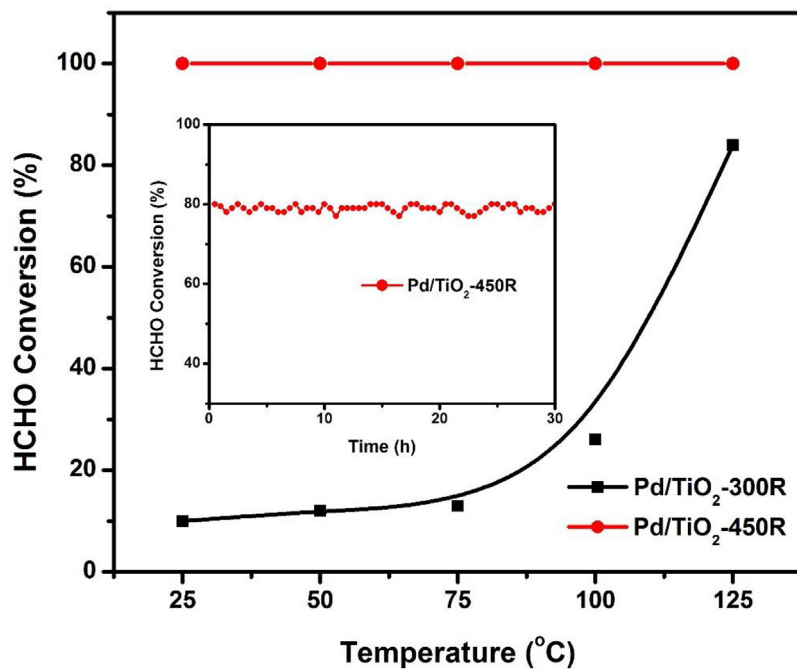


Fig. 1. HCHO conversion over Pd/TiO₂-300R and Pd/TiO₂-450R catalysts. Reaction conditions: 140 ppm HCHO, 20% O₂, 40% RH, He balance, GHSV 95000 h⁻¹. (Inset: Stability test of Pd/TiO₂-450R catalyst at room temperature with 300 ppm HCHO and other conditions as above.).

Table 1
Specific surface area (S_{BET}), Pd dispersion (D_{co}), Pd mean particle size (d_s), TOF, relative amount of surface OH groups (Ti-OH) and ratio of Pd⁰/Pd²⁺ for Pd/TiO₂-300R and Pd/TiO₂-450R catalysts together with TiO₂.

	S_{BET} (m ² /g)	D_{co} ^a (%)	d_s (nm)	TOFx10 ⁻² ^b (s)	Ti-OH ^c (%)	Pd ⁰ /Pd ²⁺ ^d
TiO ₂	58.3					
Pd/TiO ₂ -300R	57.2	21.4	4.9	0.18	14.9	1.65
Pd/TiO ₂ -450R	58.0	16.9	3.8	13.5	23.3	1.76

^a Pd dispersion measured with CO pulse chemisorption.

^b Turnover frequencies (TOF) calculated from D_{co} .

^c Concentration of Ti-OH calculated from the XPS of O 1s.

^d Concentration of Pd⁰/Pd²⁺ calculated from the XPS of Pd 3d.

3. Results and discussion

3.1. Activity in HCHO oxidation

The performance of Pd/TiO₂-300R and Pd/TiO₂-450R for HCHO oxidation was tested and the results are shown in Fig. 1. For the Pd/TiO₂-300R catalyst, only 10% HCHO conversion was achieved at room temperature and 85% HCHO conversion at 125 °C. In contrast, 100% HCHO conversion was achieved on Pd/TiO₂-450R in the investigated temperature range of 25–125 °C. The carbon balance results (Table S1) showed that the HCHO were selectively converted into CO₂ and H₂O, and no by-products was produced. Moreover, the Pd/TiO₂-450R catalyst exhibited an excellent stability, maintaining 80% conversion of 300 ppm HCHO for 30 h (insert in Fig. 1). These results showed that the Pd/TiO₂ reduced at 450 °C was much more active for HCHO oxidation than that reduced at 300 °C.

3.2. Characterization of catalysts

3.2.1. Structural features of catalysts

The XRD patterns of reduced Pd/TiO₂ catalysts and TiO₂ are shown in Fig. 2. No diffraction peaks of Pd species, including Pd⁰ or PdO, were observed on the Pd/TiO₂ catalysts, indicating that the Pd species are highly dispersed on the catalyst surface. The specific surface area (S_{BET}) results for Pd/TiO₂-300R and Pd/TiO₂-450R are listed in Table 1. The two catalysts showed similar specific surface

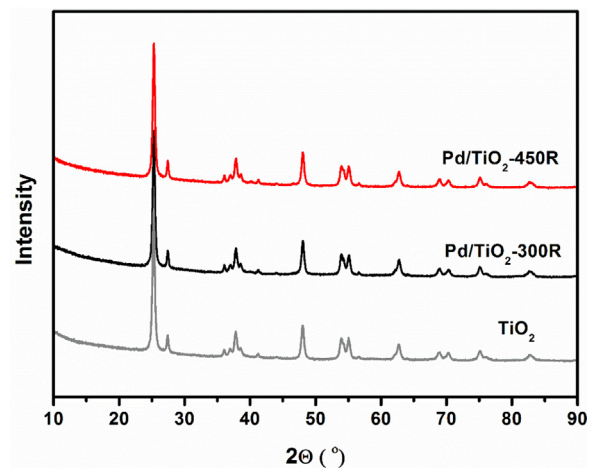


Fig. 2. XRD patterns of Pd/TiO₂-300R and Pd/TiO₂-450R catalysts together with TiO₂ sample.

areas, indicating that reduction processing had little effect on the physical properties of the catalysts.

3.2.2. Pd dispersion and particle size

CO pulsed chemisorption was used to determine the Pd dispersion (D_{co}), and the results are listed in Table 1. The Pd dispersion was

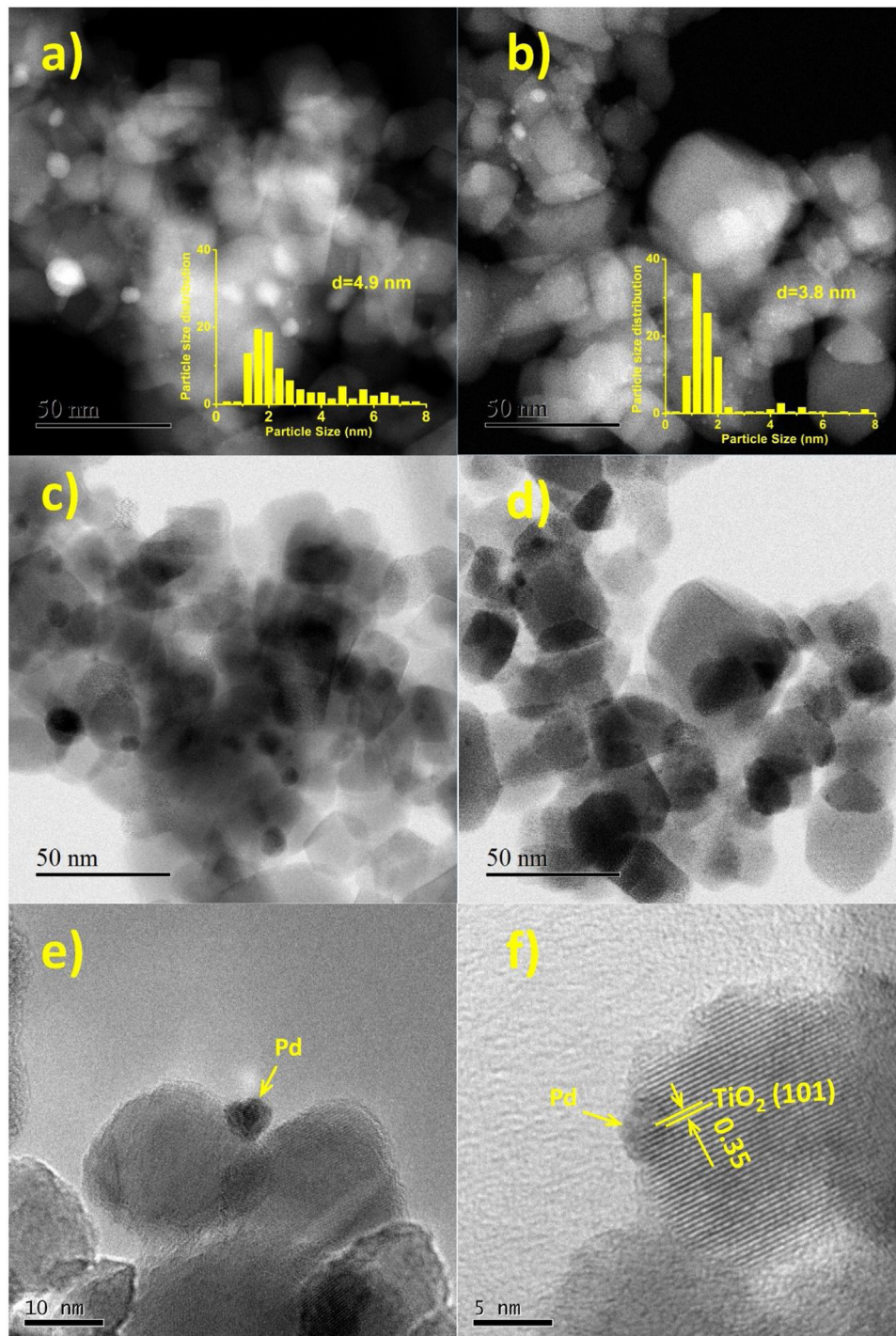


Fig. 3. HAADF/STEM images and particle size distribution of Pd/TiO₂-300R (a, dark field; c, bright field; e, HRTEM) and Pd/TiO₂-450R (b, dark field; d, bright field; f, HRTEM) samples.

21.4% on the Pd/TiO₂-300R catalyst, while the Pd dispersion was decreased to 16.9% on the Pd/TiO₂-450R catalyst, which should be attributed to agglomeration of Pd particles [32]. To verify the above speculation, HAADF/STEM measurements were carried out to observe the variation in Pd particle size. The HAADF/STEM images and Pd particle size distribution of Pd/TiO₂-300R and Pd/TiO₂-450R are shown in Fig. 3. There was little difference between the results of dark field and bright field images of Pd/TiO₂-300R (Fig. 3a and 3c) or Pd/TiO₂-450R (Fig. 3b and 3d) catalysts. The average particle size (d_s) was 4.9 nm on the Pd/TiO₂-300R catalyst. Contrary to expec-

tations, the Pd particle size on Pd/TiO₂-450R catalyst decreased to 3.8 nm, rather than increasing. This kind of abnormal phenomenon has been also observed on a CeO₂-Pt/La-Al₂O₃ catalyst calcined at high temperature, resulting from Pt nanoparticles being trapped by the support when undergoing sintering at elevated temperatures, which is known as a type of strong metal-support interaction (SMSI) [40]. According to previous works, it is believed that supported metals with large surface energies (such as Pt, Pd and Rh) could be easily encapsulated by reduced oxides with small surface energies (such as TiO_{2-x} and CeO_{2-x}), especially when reduced at

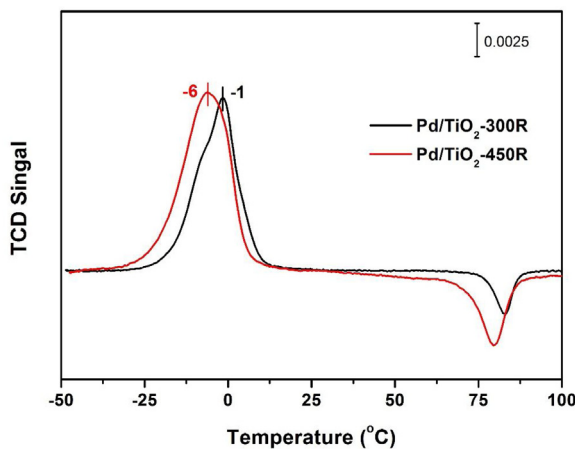


Fig. 4. $\text{H}_2\text{-TPR}$ profiles of $\text{Pd}/\text{TiO}_2\text{-300R}$ and $\text{Pd}/\text{TiO}_2\text{-450R}$ samples.

high temperature [41,42]. Comparing this result with the HRTEM image of $\text{Pd}/\text{TiO}_2\text{-300R}$ (Fig. 3e), it is obvious that partial encapsulation of Pd particles by TiO_2 had occurred on the $\text{Pd}/\text{TiO}_2\text{-450R}$ catalyst (Fig. 3f) [43]. It is well known that encapsulation could lead to the suppression of adsorption of small molecules such as CO and H_2 on the supported metals [44–46]. Therefore, in the present work, the decrease of Pd particle size could be ascribed to the following phenomenon: at high reduction temperature, reduced TiO_2 (TiO_{2-x}) diffused, partially encapsulated and finally trapped the Pd particles. Accordingly, it is easy to understand the seeming contradiction between the decrease in CO chemisorption and increase in Pd dispersion.

Based on the results of Pd dispersion, the turnover frequencies (TOF) over the two catalysts were calculated at 25 °C, and the results are summarized in Table 1. The $\text{Pd}/\text{TiO}_2\text{-300R}$ and $\text{Pd}/\text{TiO}_2\text{-450R}$ catalysts presented TOF of 0.18×10^{-2} and $13.5 \times 10^{-2} \text{ s}^{-1}$, respectively. It is clear that the high temperature reduction significantly enhanced the activity of the $\text{Pd}/\text{TiO}_2\text{-450R}$ catalyst, with a TOF 70 times higher than the $\text{Pd}/\text{TiO}_2\text{-300R}$ catalyst.

3.2.3. $\text{H}_2\text{-TPR}$

The effect of reduction temperature on the reducibility of the catalysts was investigated by $\text{H}_2\text{-TPR}$ measurements, and the results are shown in Fig. 4. The catalysts exhibited two peaks in the temperature range of $-50\text{--}100$ °C. The negative peak at around 80 °C can be assigned to hydrogen spillover [47] and the other peak at -1 °C on $\text{Pd}/\text{TiO}_2\text{-300R}$ catalyst and at -6 °C on $\text{Pd}/\text{TiO}_2\text{-450R}$ catalyst should be the reduction of surface chemisorbed oxygen species, indicating that the catalyst reducibility was enhanced after the high temperature reduction. Moreover, $\text{Pd}/\text{TiO}_2\text{-450R}$ possessed more chemisorbed O_2 according to the area of H_2 consumption.

3.2.4. XPS studies

To demonstrate the electron states of Pd and O elements on the catalyst surface, XPS measurements were carried out next, and the results are shown in Fig. 5. As shown in Fig. 5a, two kinds of Pd species were observed on both $\text{Pd}/\text{TiO}_2\text{-300R}$ and $\text{Pd}/\text{TiO}_2\text{-450R}$ catalysts. The peak located at 336.5 eV should be assigned to PdO [48], which may be attributed to the re-oxidation of metal Pd particles by O_2 and/or H_2O in air during transfer of the sample to the XPS chamber [37]. The peak at 335.1 eV on the $\text{Pd}/\text{TiO}_2\text{-300R}$ catalyst and 334.7 eV on the $\text{Pd}/\text{TiO}_2\text{-450R}$ catalyst can be ascribed to metallic Pd [49]. It can be observed that a negative shift in Pd binding energy occurred on the $\text{Pd}/\text{TiO}_2\text{-450R}$ catalyst, which could be

attributed to the increase in the electron density of the metal [50]. It was reported that more oxygen defects (TiO_{2-x}) could be obtained on the Pd/TiO_2 catalyst during the high temperature reduction process, [42] which facilitates the electron transfer from the TiO_{2-x} to the metallic Pd [51,52] and then leads to electron enrichment on the Pd particles. As a result, O_2 adsorption on Pd can be enhanced through back donation of electrons from Pd species to the anti-bonding π^* orbital of O_2 [17,53]. The distribution ratio of $\text{Pd}^0/\text{Pd}^{2+}$ on the two catalysts was calculated and the results are presented in Table 1. The two catalysts possessed similar ratio of $\text{Pd}^0/\text{Pd}^{2+}$, therefore HCHO decomposition was not affected by the distribution ratio of $\text{Pd}^0/\text{Pd}^{2+}$. As shown in Fig. 5b, the catalysts contained two kinds of O species. The main peak centered at 529.7 eV can be assigned to the lattice oxygen of bulk TiO_2 and the shoulder peak at 531.4 eV can be ascribed to the surface OH species (Ti-OH) [15,54]. The relative ratio of Ti-OH species was calculated, and the result is listed in Table 1. The percentage of Ti-OH was 14.9% on the $\text{Pd}/\text{TiO}_2\text{-300R}$ catalyst, while it markedly increased to 23.3% on the $\text{Pd}/\text{TiO}_2\text{-450R}$ catalyst. The phenomenon was also demonstrated by the results of FTIR measurements on the dry samples (Fig. S2). The peaks at 3430 cm^{-1} and 1628 cm^{-1} are assigned to the stretching and bending vibrations of surface OH, respectively [25,27]. It is obvious that $\text{Pd}/\text{TiO}_2\text{-450R}$ catalyst possesses more surface OH groups than $\text{Pd}/\text{TiO}_2\text{-300R}$ catalyst. It has been reported that surface OH groups are formed by water dissociation on oxygen vacancies [36,55,56] or on metal surfaces through water-oxygen interaction [57–59]. The OH species could facilitate O_2 adsorption and activation on TiO_2 (110) [17,60] and enhance the diffusion of oxygen along the surface Ti (5c) to the metal-support interface, which has long been recognized as the active site. [60,61]. We next carried out the $\text{O}_2\text{-TPD}$ and the results are shown in Fig. S1. It is clear that $\text{Pd}/\text{TiO}_2\text{-450R}$ catalyst possessed more chemisorbed O_2 than $\text{Pd}/\text{TiO}_2\text{-300R}$ catalyst, and the O_2 desorption temperature shifted to lower temperature by about 30 °C, further confirming a higher mobility of chemisorbed O_2 on $\text{Pd}/\text{TiO}_2\text{-450R}$ catalyst. In addition, the surface OH could accelerate the partial oxidation of HCHO to formate and also could directly react with formate species to finally produce CO_2 and H_2O at ambient temperature [13,15].

3.2.5. The role of H_2O on the $\text{Pd}/\text{TiO}_2\text{-300R/450R}$ catalysts

To clarify the role of surface OH groups in HCHO oxidation, the performance of the catalysts was also investigated with H_2O startup-shutdown cycling, and results are shown in Fig. 6. As shown in Fig. 6a, whether the reaction gas contained H_2O or not, the $\text{Pd}/\text{TiO}_2\text{-300R}$ catalyst showed a very low activity, with only 10%

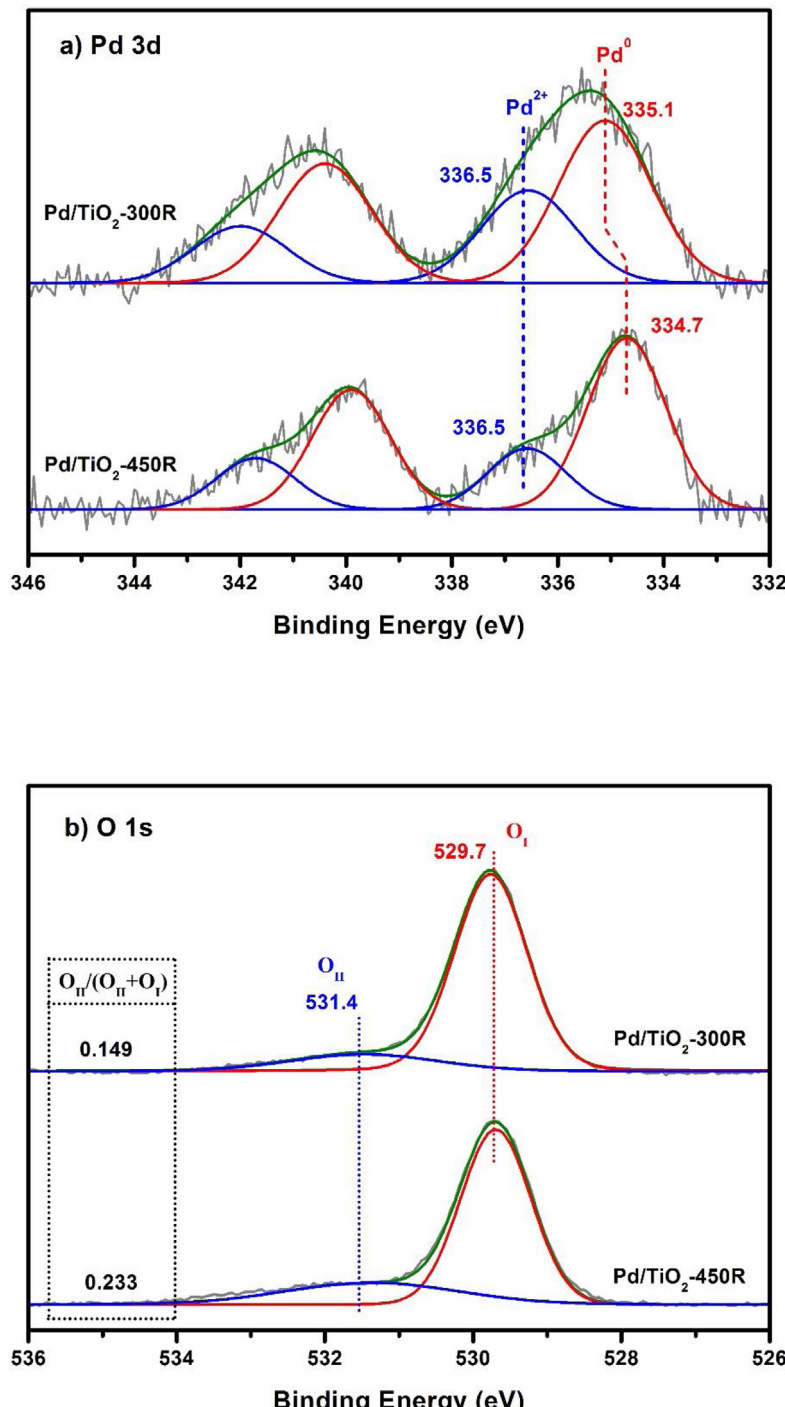


Fig. 5. XPS spectra of Pd/TiO₂-300R and Pd/TiO₂-450R samples: (a) Pd 3d (insert: Distribution ratio of Pd⁰/Pd²⁺), (b) O 1s.

HCHO conversion and little CO₂ generation, indicating that H₂O had little effect on HCHO oxidation for the Pd/TiO₂-300R catalyst. In contrast, when the Pd/TiO₂-450R catalyst (Fig. 6b) was exposed to a gas flow of 300 ppm HCHO/He/H₂O (RH=40%)/O₂ (zone 1), about 80% HCHO conversion was achieved. After 2 h without any deactivation, the H₂O was shut off (zone 2), and then HCHO conversion sharply dropped to 20%. When H₂O was re-introduced into the gas flow (zone 3), the activity of Pd/TiO₂-450R was completely recovered. Next, the activity sharply decreased again following the removal of H₂O (zone 4). The above findings showed that H₂O has a promotion effect on the Pd/TiO₂-450R catalyst for HCHO oxidation,

confirming that the surface hydroxyl group plays an important role in HCHO oxidation, and that it could be effectively recovered on the Pd/TiO₂-450R catalyst.

3.2.6. The reaction pathways of HCHO oxidation on the Pd/TiO₂-300R/450R catalysts

To identify the intermediates formed on the Pd/TiO₂-300R and Pd/TiO₂-450R catalysts at room temperature, *in situ* DRIFTS spectra were collected in a flow of 140 ppm HCHO/He/H₂O (RH=40%)/20% O₂, and the results are shown in Fig. 7. Two major surface species were observed on the Pd/TiO₂-300R catalyst (Fig. 7a), including

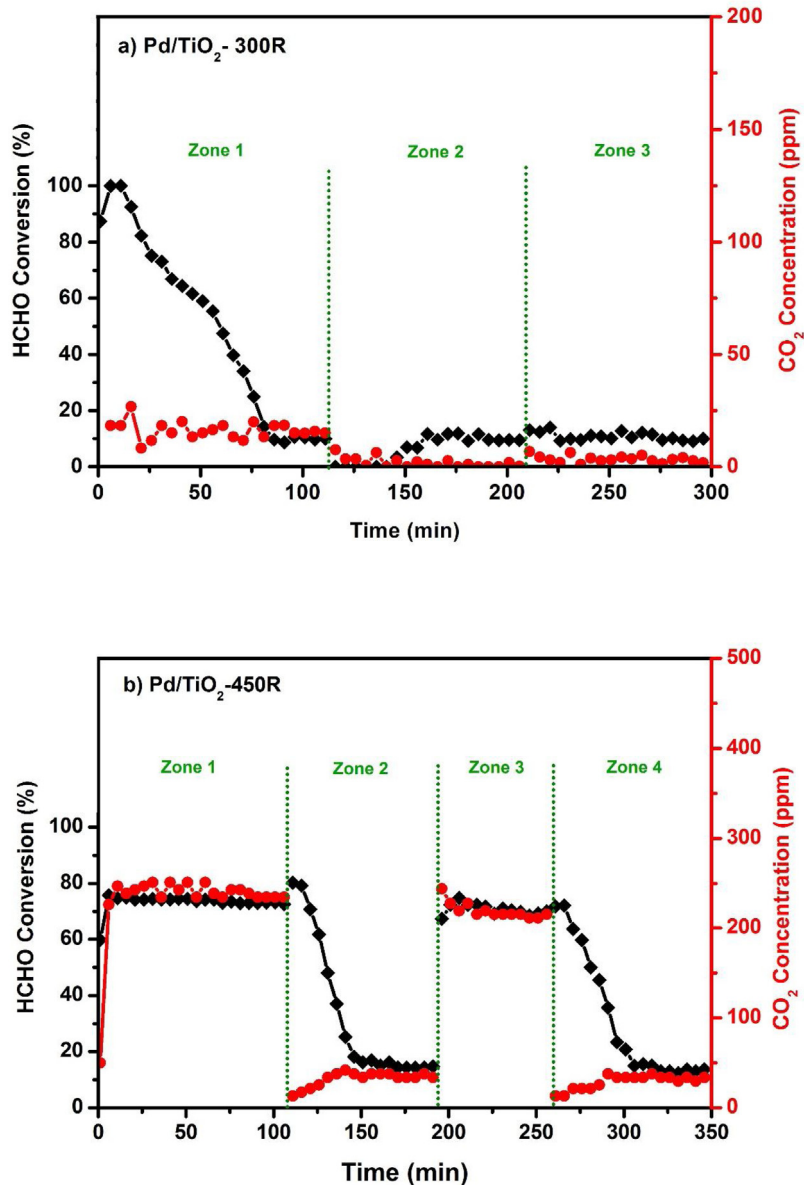


Fig. 6. H₂O effect on the activity of a) Pd/TiO₂-300R catalyst (zone 1 and 3, HCHO+He+O₂+H₂O; zone 2, HCHO+He+O₂) and b) Pd/TiO₂-450R catalyst (zone 1 and 3, HCHO+He+O₂+H₂O; zone 2 and 4, HCHO+He+O₂). Reaction conditions: 300 ppm HCHO, 20% O₂, 40% RH, He balance, GHSV 95000 h⁻¹.

adsorbed water (3327 cm⁻¹ for $\nu(\text{OH})$ and 1645 cm⁻¹ for $\delta(\text{H}_2\text{O})$) and bidentate formate (2865, 2740 cm⁻¹ for $\nu(\text{CH})$ and 1582, 1359 cm⁻¹ for $\nu(\text{COO})$) [62,63]. Meanwhile, peaks for the two species (3327, 1652 cm⁻¹ for adsorbed water and 2870, 2760, 1576, 1352 cm⁻¹ for surface formate) were also obtained on the Pd/TiO₂-450R catalyst (Fig. 7b). However, no peaks associated with molecular HCHO were observed on either of the catalysts, since it could be immediately oxidized by the surface oxygen or OH after its adsorption [13,27,38,62,64], which can be described as follows:



Therefore, the formate species were considered to be the main intermediate of HCHO oxidation. It is worth noting that the rate of formate accumulation on the Pd/TiO₂-450R catalyst was much slower than that on Pd/TiO₂-300R, indicating that the formate species could be more effectively oxidized on the Pd/TiO₂-450R catalyst [23].

HCHO-TPD was further carried out to investigate the mechanism of HCHO oxidation on Pd/TiO₂ catalysts treated by low and

high temperature reduction. The HCHO-TPD profiles are shown in Fig. 8. As shown in Fig. 8a, a broad desorption peak of CO was observed on the Pd/TiO₂-300R catalyst, starting at 60 °C and reaching a maximum at 110 °C. A CO₂ desorption peak was also obtained starting at 35 °C, and it gradually reached its maximum along with the decrease and disappearance of the CO desorption peak. Meanwhile, a small amount of H₂ was also observed in the range of 35–230 °C, which may due to the water-gas-shift reaction between CO and the limited number of surface OH groups [65,66]. The above results indicated that CO was another main intermediate, due to the decomposition of surface formate during HCHO oxidation on the Pd/TiO₂-300R catalyst, and it could further be oxidized by the surface oxygen species to form CO₂ [14,38]. The main process can be described as follows:



In comparison, only the CO₂ desorption (45–290 °C) was observed on the Pd/TiO₂-450R catalyst (Fig. 8b) with no desorption peak associated with CO or H₂ detected in the examined tempera-

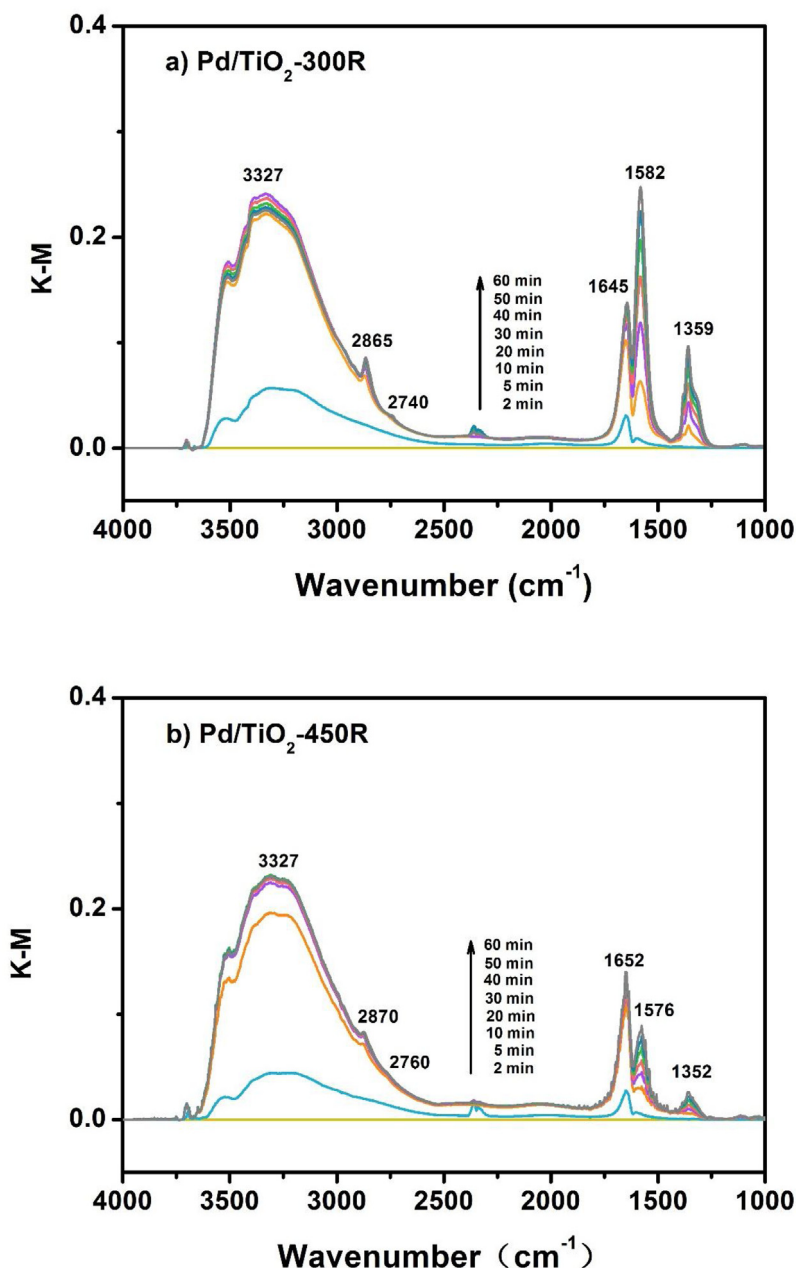


Fig. 7. *in situ* DRIFT spectra of HCHO adsorption on a) Pd/TiO₂-300R and b) Pd/TiO₂-450R samples at room temperature. Reaction conditions: 140 ppm HCHO, 20% O₂, 40% RH, He balance.

ture range, indicating that there may be a more effective pathway for the direct oxidation of surface formate. According to the previous works, the formate species could be easily and directly oxidized by surface OH groups to form CO₂ and H₂O [13,23,67,68]. The Pd/TiO₂-450R catalyst contained more surface OH groups and also was efficient for its recovery. Therefore, the HCHO oxidation on the Pd/TiO₂-450R catalyst should follow a new pathway of direct formate oxidation by OH groups as described in equation (3).



4. Conclusions

It was found that the Pd/TiO₂ reduced at 450 °C possessed a TOF 70 times higher than the Pd/TiO₂-300R catalyst, and 100% con-

version of 140 ppm HCHO could be reached on Pd/TiO₂-450R in a GHSV of 95000 h⁻¹ at room temperature. The SMSI induced by high temperature reduction could partially encapsulate the Pd particles, resulting in a smaller particle size on the catalyst surface, and subsequently promoting the activation of O₂. In addition, the partial reduction of TiO₂ at high temperature resulted in more oxygen defects and further enhanced the dissociation of H₂O to form abundant surface OH groups. The surface formate formed by partial oxidation of HCHO could be directly oxidized into the final products CO₂ and H₂O by surface OH groups on the Pd/TiO₂-450 catalyst. In contrast, HCHO oxidation on Pd/TiO₂-300R followed a slower pathway of formate decomposition to CO. Hence, the Pd/TiO₂-450R catalyst exhibits much higher activity than Pd/TiO₂-300R for HCHO oxidation at room temperature.

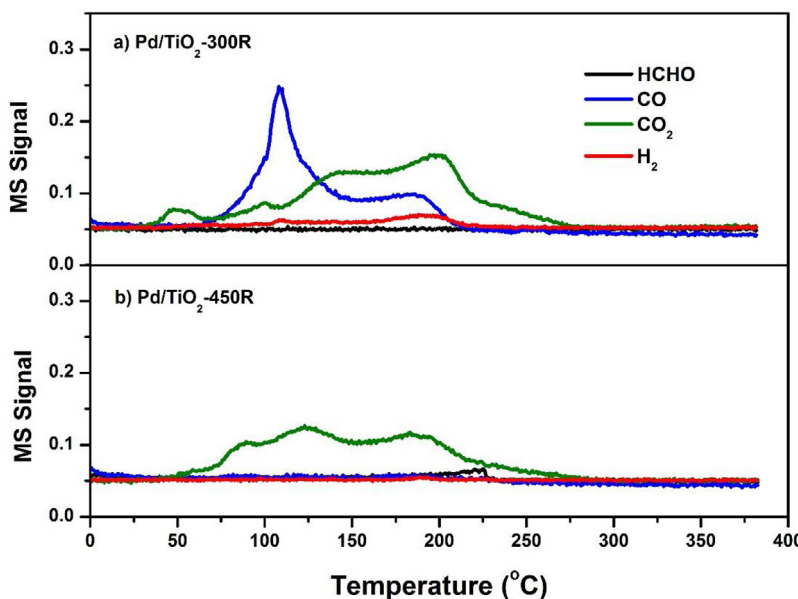


Fig. 8. HCHO-TPD profiles of a) Pd/TiO_2 -300R and b) Pd/TiO_2 -450R samples.

Acknowledgments

This work was financially supported by the National Natural Science Foundation of China (21422706, 21577159, 51608504).

Appendix A. Supplementary data

Supplementary data associated with this article can be found, in the online version, at <http://dx.doi.org/10.1016/j.apcatb.2017.06.023>.

References

- [1] W.H. Liang, X.D. Yang, *Build. Environ.* 69 (2013) 114–120.
- [2] G.D. Nielsen, S.T. Larsen, P. Wolkoff, *Arch Toxicol.* 87 (2013) 73–98.
- [3] F. Shiraishi, D. Ohkubo, K. Toyoda, S. Yamaguchi, *Chem. Eng. J.* 114 (2005) 153–159.
- [4] C.H. Ao, S.C. Lee, *Appl. Catal. B* 44 (2003) 191–205.
- [5] F. Holzer, U. Roland, F.D. Kopinke, *Appl. Catal. B* 38 (2002) 163–181.
- [6] M.B. Chang, C.C. Lee, *Environ. Sci. Technol.* 29 (1995) 181–186.
- [7] J. Quiroz Torres, S. Royer, J.P. Bellat, J.M. Giraudon, J.F. Lamonier, *Chemsuschem* 6 (2013) 578–592.
- [8] J.J. Pei, J.S.S. Zhang, *Hvac & R Res.* 17 (2011) 476–503.
- [9] P.P. Hu, Z. Amghouz, Z.W. Huang, F. Xu, Y.X. Chen, X.F. Tang, *Environ. Sci. Technol.* 49 (2015) 2384–2390.
- [10] X.F. Tang, Y.G. Li, X.M. Huang, Y.D. Xu, H.Q. Zhu, J.G. Wang, W.J. Shen, *Appl. Catal. B* 62 (2006) 265–273.
- [11] J. Quiroz, J.M. Giraudon, A. Gervasini, C. Dujardin, C. Lancelot, M. Trentesaux, J.F. Lamonier, *ACS Catal.* 5 (2015) 2260–2269.
- [12] B.Y. Bai, H. Arandian, J.H. Li, *Appl. Catal. B* 142 (2013) 677–683.
- [13] C.B. Zhang, F.D. Liu, Y.P. Zhai, H. Ariga, N. Yi, Y.C. Liu, K. Asakura, M. Flytzani-Stephanopoulos, H. He, *Angew. Chem. Int. Ed.* 51 (2012) 9628–9632.
- [14] S.S. Kim, K.H. Park, S.C. Hong, *Appl. Catal. A* 398 (2011) 96–103.
- [15] D.W. Kwon, P.W. Seo, G.J. Kim, S.C. Hong, *Appl. Catal. B* 163 (2015) 436–443.
- [16] H.F. Li, N. Zhang, P. Chen, M.F. Luo, J.Q. Lu, *Appl. Catal. B* 110 (2011) 279–285.
- [17] H.B. Huang, D.Y.C. Leung, *ACS Catal.* 1 (2011) 348–354.
- [18] E. Jeroro, J.M. Vohs, *J. Am. Chem. Soc.* 130 (2008) 10199–10207.
- [19] C.B. Zhang, Y.B. Li, Y.F. Wang, H. He, *Environ. Sci. Technol.* 48 (2014) 5816–5822.
- [20] S. Imamura, Y. Uematsu, K. Utani, T. Ito, *Ind. Eng. Chem. Res.* 30 (1991) 18–21.
- [21] Q. Xu, W. Lei, X. Li, X. Qi, J. Yu, G. Liu, J. Wang, P. Zhang, *Environ. Sci. Technol.* 48 (2014) 9702–9708.
- [22] Y.B. Li, C.B. Zhang, H. He, J.H. Zhang, M. Chen, *Catal. Sci. Technol.* 6 (2016) 2289–2295.
- [23] B.B. Chen, C. Shi, M. Crocker, Y. Wang, A.M. Zhu, *Appl. Catal. B* 132 (2013) 245–255.
- [24] S.J. Park, I. Bae, I.S. Nam, B.K. Cho, S.M. Jung, J.H. Lee, *Chem. Eng. J.* 195 (2012) 392–402.
- [25] Z.H. Xu, J.G. Yu, M. Jaroniec, *Appl. Catal. B* 163 (2015) 306–312.
- [26] Z.X. Yan, Z.H. Xu, J.G. Yu, M. Jaroniec, *Appl. Catal. B* 199 (2016) 458–465.
- [27] T.F. Yang, Y. Huo, Y. Liu, Z.B. Rui, H.B. Ji, *Appl. Catal. B* 200 (2017) 543–551.
- [28] H.Y. Chen, M.N. Tang, Z.B. Rui, H.B. Ji, *Ind. Eng. Chem. Res.* 54 (2015) 8900–8907.
- [29] H.Y. Tan, J. Wang, S.Z. Yu, K.B. Zhou, *Environ. Sci. Technol.* 49 (2015) 8675–8682.
- [30] J.D. Bracey, R. Burch, *J. Catal.* 86 (1984) 384–391.
- [31] Y.A. Ryndin, M.V. Stenin, A.I. Boronin, V.I. Bukhtiyarov, V.I. Zaikovskii, *Appl. Catal.* 54 (1989) 277–288.
- [32] C.A. Muller, M. Maciejewski, R.A. Koeppe, A. Baiker, *J. Catal.* 166 (1997) 36–43.
- [33] S.Y. Huang, C.B. Zhang, H. He, *J. Environ. Sci.* 25 (2013) 1206–1212.
- [34] H.B. Huang, P. Hu, H.L. Huang, J.D. Chen, X.G. Ye, D.Y.C. Leung, *Chem. Eng. J.* 252 (2014) 320–326.
- [35] H.L. Tang, J.K. Wei, F. Liu, B.T. Qiao, X.L. Pan, L. Li, J.Y. Liu, J.H. Wang, T. Zhang, *J. Am. Chem. Soc.* 138 (2016) 56–59.
- [36] I. Brookes, C. Muryn, G. Thornton, *Phys. Rev. Lett.* 87 (2001) 1–4.
- [37] X.L. Zhu, M. Shen, L.L. Lobban, R.G. Mallinson, *J. Catal.* 278 (2011) 123–132.
- [38] C. Zhang, H. He, K.-i. Tanaka, *Appl. Catal. B* 65 (2006) 37–43.
- [39] P. Panagiotopoulou, D.I. Koniarides, *J. Catal.* 225 (2004) 327–336.
- [40] J. Jones, H.F. Xiong, A.T. Delariva, E.J. Peterson, H. Pham, S.R. Challa, G.S. Qi, S. Oh, M.H. Wiebenga, X.I.P. Hernandez, Y. Wang, A.K. Datye, *Science* 353 (2016) 150–154.
- [41] Q. Fu, T. Wagner, S. Olliges, H.D. Carstanjen, *J. Phys. Chem. B* 109 (2005) 944–951.
- [42] Y.Z. Li, B.L. Xu, Y.N. Fan, N.Y. Feng, A.D. Qiu, J.M.J. He, H.P. Yan, Y. Chen, *J. Mol. Catal. A* 216 (2004) 107–114.
- [43] H.P. Sun, X.P. Pan, G.W. Graham, H.W. Jen, R.W. McCabe, S. Thevuthasan, C.H.F. Peden, *Appl. Phys. Lett.* 87 (2005).
- [44] S.J. Tauster, S.C. Fung, R.L. Garten, *J. Am. Chem. Soc.* 100 (1978) 170–175.
- [45] M.A. Vannice, C.C. Twu, S.H. Moon, *J. Catal.* 79 (1983) 70–80.
- [46] E.V. Benvenutti, L. Franken, C.C. Moro, C.U. Davanzo, *Langmuir* 15 (1999) 8140–8146.
- [47] R. Prins, *Chem. Rev.* 112 (2012) 2714–2738.
- [48] K. Otto, L.P. Haack, J.E. deVries, *Appl. Catal. B* 1 (1992) 1–12.
- [49] H.Q. Yang, G.Y. Zhang, X.L. Hong, Y.Y. Zhu, *J. Mol. Catal. A* 210 (2004) 143–148.
- [50] L.F. Liotta, G.A. Martin, D. Deganello, *J. Catal.* 164 (1996) 322–333.
- [51] M.A. Aramendia, J.C. Colmenares, A. Marinas, J.M. Marinas, J.M. Moreno, J.A. Navio, F.J. Urbano, *Catal. Today* 128 (2007) 235–244.
- [52] Z.B. Rui, L.Y. Chen, H.Y. Chen, H.B. Ji, *Ind. Eng. Chem. Res.* 53 (2014) 15879–15888.
- [53] C.G. Vayenas, S. Bebelis, C. Pliangos, S. Brosda, D. Tsipakides, Kluwer Academic Publishers/Plenum New Press York, 2001, pp. 35–86.
- [54] L.H. Nie, J.G. Yu, X.Y. Li, B. Cheng, G. Liu, M. Jaroniec, *Environ. Sci. Technol.* 47 (2013) 2777–2783.
- [55] Z. Zhang, O. Bondarchuk, B.D. Kay, J.M. White, Z. Dohnalek, *J. Phys. Chem. B* 110 (2006) 21840–21845.
- [56] A. Vecchietti, W.Q. Bonivardi, D. Xu, J.J. Stacchiola, M. Calatayud, S.E. Collins, *ACS Catal.* 4 (2014) 2088–2096.
- [57] R.A. Ojifinni, N.S. Froemming, J. Gong, M. Pan, T.S. Kim, J.M. White, G. Henkelman, C.B. Mullins, *J. Am. Chem. Soc.* 130 (2008) 6801–6812.
- [58] A. Bongiorno, U. Landman, *Phys. Rev. Lett.* 95 (2005) 1–4.
- [59] T.S. Kim, J. Gong, R.A. Ojifinni, J.M. White, C.B. Mullins, *J. Am. Chem. Soc.* 128 (2006) 6282–6283.

[60] L.M. Liu, B. McAllister, H.Q. Ye, P. Hu, J. Am. Chem. Soc. 128 (2006) 4017–4022.

[61] S.C. Ammal, A. Heyden, ACS Catal. 4 (2014) 3654–3662.

[62] Y.B. He, H.B. Ji, Chinese J. Catal. 31 (2010) 171–175.

[63] Z. Chang, G. Thornton, Surf. Sci. 459 (2000) 303–309.

[64] H. Idriss, K.S. Kim, M.A. Barteau, Surf. Sci. 262 (1992) 113–127.

[65] C. Ratnasamy, J.P. Wagner, Catal. Rev. 51 (2009) 325–440.

[66] Y.P. Zhai, D. Pierre, R. Si, W. Deng, P. Ferrin, A.U. Nilekar, G.W. Peng, J.A. Herron, D.C. Bell, H. Saltsburg, M. Mavrikakis, M. Flytzani-Stephanopoulos, Science 329 (2010) 1633–1636.

[67] K. Tanaka, M. Shou, H. He, X.Y. Shi, X.L. Zhang, J. Phys. Chem. C 113 (2009) 12427–12433.

[68] B.Y. Bai, J.H. Li, ACS Catal. 4 (2014) 2753–2762.